Published in final edited form as:
Lab Invest. 2010 May ; 90(5): 774–786. doi:10.1038/labinvest.2010.6.

Hippocampal CA1 atrophy and synaptic loss during experimental autoimmune encephalomyelitis, EAE

Marina O Ziehn[1,2], **Andrea A Avedisian**[2], **Seema Tiwari-Woodruff**[2], and **Rhonda R Voskuhl**[2]

[1]Interdepartmental Program of Neuroscience, University of California, Los Angeles, CA, USA

[2]Multiple Sclerosis Program, Department of Neurology, University of California, Los Angeles, CA, USA

Abstract

Over half of multiple sclerosis (MS) patients experience cognitive deficits, including learning and memory dysfunction, and the mechanisms underlying these deficits remain poorly understood. Neuronal injury and synaptic loss have been shown to occur within the hippocampus in other neurodegenerative disease models, and these pathologies have been correlated with cognitive impairment. Whether hippocampal abnormalities occur in MS models is unknown. Using experimental autoimmune encephalomyelitis (EAE), we evaluated hippocampal neurodegeneration and inflammation during disease. Hippocampal pathology began early in EAE disease course, and included decreases in CA1 pyramidal layer volume, loss of inhibitory interneurons and increased cell death of neurons and glia. It is interesting to note that these effects occurred in the presence of chronic microglial activation, with a relative paucity of infiltrating blood-borne immune cells. Widespread diffuse demyelination occurred in the hippocampus, but there was no significant decrease in axonal density. Furthermore, there was a significant reduction in pre-synaptic puncta and synaptic protein expression within the hippocampus, as well as impaired performance on a hippocampal-dependent spatial learning task. Our results demonstrate that neurodegenerative changes occur in the hippocampus during autoimmune-mediated demyelinating disease. This work establishes a preclinical model for assessing treatments targeted toward preventing hippocampal neuropathology and dysfunction in MS.

Keywords

EAE; hippocampus; MS; pathology

Multiple sclerosis (MS) is a chronic inflammatory, neurodegenerative disease, with onset at ages 20–40 years in young adults who have a normal lifespan. Autoimmune responses directed against myelin are thought to be involved in the immunopathogenesis of MS.1 It is classically considered a white matter (WM) demyelinating disease, characterized by focal WM lesions consisting of T lymphocyte and macrophage infiltrates, demyelination and axonal transection.2–4 However, WM pathology does not occur exclusively. Gray matter atrophy has been shown to occur in cortical and deep sub-cortical brain regions by magnetic

Correspondence: Dr RR Voskuhl, MD, Department of Neurology, University of California, Neuroscience Research Building 1, Room 475D, 635 Charles E Young Drive South, Los Angeles, CA 90095, USA. rvoskuhl@ucla.edu.

DISCLOSURE/CONFLICT OF INTEREST
The authors declare no conflict of interest.

resonance imaging (MRI).5–8 Gray matter atrophy begins early in the disease, continues as the disease progresses,9 and correlates with motor, sensory and visual disability as well as with cognitive deficits.10 Indeed, approximately 50–65% of MS patients experience cognitive deficits.[11,12] Among these reported cognitive deficits, memory dysfunction is especially common. [13] The cause of memory dysfunction in MS is currently unknown, but neuroimaging studies suggest that hippocampal pathology is involved,[14] specifically, atrophy of the CA1 region.[15]

Experimental autoimmune encephalomyelitis (EAE) is the most commonly used animal model of MS. Like MS, EAE is characterized by inflammation and neurodegeneration in the spinal cord and the brain. How these two processes interact to cause permanent disability remains unclear. In EAE, neuroinflammation and axonal loss in spinal cord has been proposed to result in walking disability.[16] In contrast, the neuropathological substrate underlying cognitive disability remains unknown. Herein we describe hippocampal neurodegeneration and consequent spatial learning impairment, in myelin oligodendrocyte glycoprotein (MOG) peptide induced EAE in C57BL/6 mice. This novel characterization of hippocampal pathology in the MS model may yield insights into the basis for learning and memory deficits in MS.

MATERIALS AND METHODS

Animals

Adult male C57Bl/6 and B6.Cg-Tg (Thy1-YFP) 16 Jrs/J mice, age 8–10 weeks, were purchased from Jackson Laboratories (Bar Harbor, ME, USA). In addition, PLP–EGFP mice were bred in house, from a breeding pair, a kind gift from Dr Wendy Macklin (Cleveland Clinic Foundation, Cleveland, OH, USA). The generation, characterization and genotyping of PLP–EGFP transgenic mice have been previously reported.17,18 All animals were housed under guidelines set by the National Institutes of Health Guide for the Care and Use of Laboratory Animals. All experiments were conducted in accordance with the University of California Los Angeles (UCLA) Chancellor's Animal Research Committee (ARC), and the PHS Policy on Humane Care and Use of Laboratory Animals.

EAE

EAE was induced by subcutaneuous injection of an emulsion containing purified auto-antigen myelin oligodendrocyte glycoprotein (MOG) peptide, amino acids 35–55 (200 μg per mouse, Chiron Mimotopes, San Diego, CA, USA), and mycobacterium tuberculosis, (200 μg per mouse) suspended in complete Freund's adjuvant, as described.[19,20] Mice were monitored daily, and clinical disease severity was measured using the standard EAE grading scale.21 The standard grading scale ranges from 0 to 5: 0, unaffected; 1, loss of tail tone; 2, limb weakness; 3, partial paralysis; 4, complete paralysis; and 5, moribund. Mice were scored daily throughout the duration of experiment. Individual clinical scores were averaged across all animals per day, yielding a mean clinical disease index for each group.

Barnes Maze Spatial Memory Test

Spatial learning was assessed in normal and EAE mice using the Barnes Maze, as described previously.22 Briefly, the Barnes Maze is spatial learning and memory task, which is less physically demanding and less stressful than the Morris Water Maze,[23] yet still requires the learned association of spatial cues to a target or escape location. We adapted the Barnes Maze, in order to avoid unnecessary physical demands and stress on EAE mice. To test spatial memory, mice were placed in the middle of an elevated circular platform, 90 cm in diameter, containing 20 holes around the periphery. Holes were identical in appearance and width, 5 cm, and separated by 7 cm. Only one hole was connected to an escape route,

consisting of a 12 cm ramp into a dark 20 × 30 × 20 cm cage lowered directly under the platform. All other holes were blocked with wire mesh. Four internal spatial cues (square-, triangle-, circle- and cross-shaped color paper cut-outs) were pasted to a black wall affixed to the periphery of the platform. None of the cues were placed directly over the target hole. To enhance the natural agoraphobia of mice, a 60W lamp was placed 3 ft above the platform, while the experiment took place in a dark room. In addition, mice were exposed to noxious auditory stimulus with the use of a metronome (Intelli Programmable Metronome IMT-400), set at 120 beats per minute in the form of eight notes with an eighth rest every other note, at 440 Hz pitch. At each trial mice were lowered onto the platform in a Start box for 20 s; then given 300 s to complete the trial. Trials were completed upon entry to target hole. Errors were defined as exploration of incorrect holes, and were counted for the duration of each trial. Total errors per trial were compared between groups. EAE mice with a clinical disability score of 2.5 or higher (limp tail, difficulty righting, ataxia and mild limb weakness) were excluded from behavioral experiment. The platform was cleaned and wiped between each trial. Mice were tested three times each day, at baseline before disease induction on days −1, 0 and 1. Then mice with similar baselines were assigned to either EAE induction or not. At day 15 and day 40 during disease, or equivalent times in healthy controls, mice underwent Barnes Maze testing. Performance was assessed by change in errors from first to last trial on each day. As motor disability occurs in EAE mice, latency times to reach target hole were measured but not analyzed, as motor disability would confound timed performance.

Tissue Collection and Sectioning

At different time points (days post immunization (dpi) 13–15, 35–40 and 55) through out the disease, EAE mice were compared with age-matched healthy control mice. Mice from each group were deeply anesthetized with isoflurane and perfused transcardially with ice-cold 0.9% saline, followed by 10% formalin. The brains were dissected from skulls, post-fixed overnight in 10% formalin and cryoprotected in 30% sucrose solution in phosphate buffered saline (PBS) thereafter. Tissue was embedded in a gelatin block for cryostat sectioning then post-fixed overnight in 10% formalin and cryoprotected in 30% sucrose solution in PBS before longitudinal bisection at the midline of the brain. Sagittal free-floating sections were cut from each hemisphere: the left cut into 40 μm, the right hemisphere cut into 20 μm thick sections, with a sliding microtome, (Microm Microtome Cryostat HM 505E, Zeiss, Germany) and collected serially in PBS. The most medial sagittal section of a given block containing a complete portion of the hippocampus was numbered as the zeroth section, with all consecutive sections numbered sequentially. The first section used for the experiment was chosen uniform randomly to employ the Cavalieri method, an unbiased estimator of object volume.[24,25] From the uniform random section on, every fifth section was collected for each immunohistochemical condition.

Immunohistochemistry

For CA1 volume estimation, five sagittal sections containing the dorsal hippocampus, spanning approximately 640 μm, (Bregma lateral coordinates 0.12 to 1.08 mm, from Paxinos Franklin Mouse Brain Atlas, 200126) were collected from each hemisphere, and placed within each well of a 24-well plate. These sections were either used for immunofluorescence or Nissl stained. For all other immunostaining conditions, three sagittal sections were used, spanning approximately 400 μm of dorsal hippocampus. For immunofluorescence, 40 μm free-floating sections were permeabilized in a 2% normal goat serum (NGS), 0.3% Triton X-100 and PBS solution, and blocked with 10% NGS in PBS. To detect specific cell types and structures, sections were incubated with primary antibodies overnight. Sections were randomly selected for immuno-staining groups. Several cell types and proteins were analyzed: CA1 pyramidal neurons, CA1 inhibitory interneurons,

microglia/macrophage, immune cell infiltrates (including T and B cells), myelin basic protein and synaptic proteins. The following antibodies were used: monoclonal anti-neuronal specific nuclear protein (NeuN; 1:250), and rabbit polyconal anti-parvalbumin (PV; 1:500, Chemicon, Temecula, CA, USA) were used to identify CA1 pyramidal neurons and a subset of GABA-ergic interneurons. Rat monoclonal anti-mouse CD45, rat monoclonal anti-mouse macrophage/monocyte (both 1:500; Chemicon), were used to identify cells of microglial/macrophage lineage. To identify potential infiltrating T and B cells, rat monoclonal anti-mouse CD3 (1:50; BD Biosciences, San Jose, CA, USA) and rat monoclonal anti-mouse CD19 (1:50; BD Biosciences) were used, respectively. Rat monoclonal anti-myelin basic protein (MBP; 1:500; Chemicon) was used to stain myelin, and rabbit polyclonal anti-synapsin-1 (Syn-1; 1:500; Chemicon) was used to stain presynaptic densities. All primary antibodies were diluted at optimal working concentrations in 2% NGS in PBS. Sections were then incubated for 2 h with fluorescent-conjugated secondary antibodies (goat anti-mouse or goat anti-rat Cy5/TritC IgG (1:1000; Chemicon) and goat anti-rabbit FIT-C IgG (1:1000; Vector Laboratories, Burlingame, CA, USA) in 2%NGS in TBS solution) to visualize monoclonal and polyclonal primary antibody immunoreactivity.

To detect apoptotic cells within the CA1, the TUNELTMR, *in situ* cell death kit (Roche Applied Science, Mannheim, Germany) was used. From each animal 20 μm-thick medial brain sections containing the dorsal CA1 were taken and placed in 1.5 ml Eppendorf tubes for TUNEL procedure. Following the Roche protocol for difficult tissue, the brain sections were washed in PBS, then permeabilized in a 0.1% sodium citrate, 0.1% triton-X100 in PBS solution for 30 min at 75 °C. After rinsing with PBS, the brain sections were incubated for 1 h with TUNEL mixed solution (1:10 dilution factor of enzyme terminal deoxyribonucleic transferase (TdT) in label solution, containing fluorescent-conjugated nucleotides) in a dark, humidified chamber held at 37 °C. The sections were then rinsed in PBS, and either incubated with primary antibodies for double-labeling experiments or stained with a cell marker. 4′, 6-diamidine-2′-pheynylindole dihydrochloride, (DAPI; 1:1000; Invitrogen, Eugene, OR, USA) staining was used in all fluorescence staining conditions to identify nuclear DNA in all cell types. Primary and secondary antibody control experiments were carried out for all staining conditions. For TUNEL staining, positive control condition included incubation with DNase enzyme (200 U/μl DNase in 50μM Tris-HCL in PBS) for 10 min, before TUNEL step. After immunohistochemical procedure, all sections were mounted in serial order on Super-Frost Plus micro slides (VWR International, West Chester, PA, USA), dried overnight and cover-slipped in Fluoromount G (Fisher Scientific, Hampton, NH, USA).

Microscopy

To avoid experimenter bias during all phases of image collection and analysis, slides were coded and experimenter was blind to animal condition. The dorsal CA1 was imaged using a spinning disc laser confocal system (Olympus BX61) equipped with × 4 and × 10 dry and × 40 and × 100 oil objectives connected to a camera (Hanamatsu 1394 ORCA-ERA). Identical light intensity and exposure settings were applied to all images taken for each experimental set.

Stereological Analysis

Immunostaining was quantified using unbiased stereology. All images (RGB) were converted to grayscale, split and separated by color channel, using ImageJ version 1.29 (Windows version of NIH Image), downloaded from http://rsb.info/nih/gov/ij. To avoid experimenter bias, auto-adjustment of brightness and contrast, as well as threshold of staining signal, was carried out by NIH software. A Grid Plug-in, uploaded from

http://rsb.info.nih.gov/ij/plugins/grid.html, was used for counting points per area of interest. 27 The volume of the dorsal CA1 was estimated using the Cavalieri method.[25] For each mouse, NeuN/Dapi co-labeling and Nissl staining was analyzed within the hippocampal region of CA1. Briefly, a grid consisting of 1 pixel thick crosses was randomly superimposed onto each single-color optical image within a stack through the CA1. The area associated with each cross point was calculated using the given area of the grid, the number of crosses per grid and the ratio of micron per pixel, (1 pixel = 0.16125 μm at × 40 magnification). The average number of crosses per area was calculated, and used to estimate volume using this formula: $V = T \cdot a/p \cdot \Sigma (P_i)$, where T is the section thickness of the tissue slice, a/p is the area associated with each cross on the grid, and P_i is the number of crosses landing within the CA1 transect on each section. Volumes were estimated for each CA1 per brain slice, and statistically compared between groups. PV-positive interneurons, CD3+, macrophage/monocyte, CD19+ cells (infiltrating T cells, macrophages and B cells), and PLP + oligodendrocytes lying within the CA1 region of the hippocampus, were counted manually using × 10 images, and compared blindly between control and EAE groups. Pixel intensity of microglial/macrophage activation, myelin and synaptic protein density within the CA1 were also measured as percent area of immunoreactivity, using ImageJ, then recorded and compared statistically. Axon density was measured by the ratio of Thy-1 YFP+ pixel intensity and the total-image pixel area. All pixel intensities were measured and compared using × 10 and × 40 images. TUNEL-labeled cells (undergoing apoptosis) were counted using ImageJ particle analysis.

Presynaptic Puncta Quantification

To quantify Syn-1 immunoreactive (Syn-1-IR) presynaptic puncta within the CA1, confocal images containing the pyramidal and proximal stratum radiatum regions were acquired at × 60 magnification, transferred to a work station and RGB split using ImageJ. Three stacks of 10–12 images were taken across the CA1, for each brain section, with two brain sections sampled for each animal, for a total of 528 optical sections measured for Syn-1-IR puncta quantification. Puncta size threshold range was determined by sampling several Syn-1-IR puncta from various animals, and averaging both upper and lower threshold limits; minimum puncta size (0.816 μm^2) and maximum puncta size (3.264 μm^2). This range was then used to filter for puncta particle size through out the experiment. The number of puncta in each optical image was averaged across *z*-stack, brain section, and animal; to attain a composite average of pre-synaptic puncta within the sampled hippocampal area in different group conditions. Experimenter was blind to group conditions through out all the analyses.

Statistical Analysis

Estimated volumes, cell counts and pixel intensity percentages were compared between normal and EAE groups using an unpaired Student's *t* test. Behavioral data was analyzed using a Repeated Measures ANOVA, and Bonferroni post-hoc tests. All statistical analyses were carried out using GraphPad Prism Version 4 (GraphPad Software, San Diego, CA, USA).

RESULTS

Neurodegeneration and Microglial Activation Occur within the Hippocampus During EAE

To determine whether the hippocampus is targeted during an autoimmune demyelinating disease, EAE was induced in C57Bl/6 mice by immunizing with myelin oligodendrocyte glycoprotein (MOG 35–55) peptide, as previously described.[19,20] Consistent with previous experiments, motor disability began approximately 8–12 days after disease induction and persisted throughout the disease, Figure 1.

The integrity of hippocampal gray matter was evaluated during EAE by assessing pyramidal CA1 volume and GABA-ergic interneuron labeling. CA1 pyramidal volume was estimated using the Cavalieri Estimator, as described.[25] As hypothesized, the volume of CA1 (as identified by NeuN+/DAPI+ co-labeling of pyramidal neurons) in EAE was significantly smaller than the CA1 of healthy matched controls, starting as early as day 13 of disease, Figure 2a–c. This result was confirmed using Nissl staining (data not shown). Furthermore, GABA-ergic interneuron numbers were significantly decreased in EAE mice at the early time point of disease, as demonstrated by PV-positive staining, Figure 2a, b and d. Similar results were found in the CA1 region of EAE mice from middle and late stages (days 35 and 55, respectively) of disease, indicating an early onset of neuronal injury, which remained chronic into later stages, Figure 2e–h, i–l. These results demonstrated that the hippocampus is targeted during autoimmune demyelinating disease.

In all the stages of disease, inflammation, identified by CD45+ immunoreactivity, was abundant in the CA1 of EAE mice compared with healthy age and gender-matched controls, Figure 3. The morphology of CD45+ staining was consistent with microglia in activated states; see insets in panels b, e and h of Figure 3. As CD45+ staining does not distinguish between resident microglia and infiltrating immune cells, we next assessed whether CD45 staining was composed of T lymphocytes, B lymphocytes or macrophage/monocytes, Figure 4. EAE mice did not have immunolabeling of T cells or B cells within the hippocampus, panels a–b and g–h. However, there was some staining of globoid-shaped macrophage/monocyte lineage cells within the hippocampus, see panels d–e. Together, these data indicated that neuroinflammation in the CA1 of EAE was primarily because of activated microglia and macrophages and not because of infiltrating T and B lymphocytes.

Neurodegeneration and inflammation of the CA1 occurred in the presence of diffuse loss of myelin protein, Figure 5a–c. Although there was a trend towards decreased axonal density and reduced mature oligodendrocyte counts in EAE, these were not significantly different from normal control CA1, panel a–f $P>0.05$.

EAE Causes Neuronal and Glial Cell Death Within the Hippocampus

Once we determined that hippocampal pathology in EAE entailed a decrease in CA1 pyramidal volume and a significant loss off GABA-ergic interneurons, in the presence of microglial activation and demyelination, we then determined if cell death was also occurring in the hippocampus of EAE mice. We found increased levels of apoptotic (TUNEL+) cells within the CA1 regions of dorsal hippocampus in EAE, compared with matched healthy control mice, Figure 6a, b, d–f. Indeed, there was an approximate two-fold increase of apoptosis in all sub-regions of the CA1 in EAE.

To determine which cell types were undergoing apoptosis in the CA1 region of the hippocampus during EAE, we co-labeled adjacent tissue sections containing the dorsal CA1, with TUNEL and cell-specific markers for neurons, GABA-ergic interneurons, astrocytes and oligodendrocytes. TUNEL+ staining co-localized with neurons, interneurons and astrocytes, but detected only occasionally in oligodendrocytes, Figure 7a–h.

Hippocampal Synaptic Integrity is Disrupted During EAE

As we found increased microglial activation in the CA1, a region known to have numerous synaptic connections, and as synaptic dysfunction in the hippocampus had been previously implicated in other neurodegenerative diseases,[28] we next investigated synaptic protein expression in the CA1 layers: stratum oriens, pyramidal and radiatum. It is interesting to note that synaptic density in EAE mice was decreased in these CA1 layers, where incoming synaptic input from Schaeffer collaterals is received by pyramidal neurons and their

correspondent dendritic arborizations. To confirm a decrease in synaptic integrity, Syn-1 immunoreactive puncta were quantified using confocal microscopy. EAE mice had significantly reduced Syn-1+ puncta in the stratum radiatum, compared with the matched healthy controls, Figure 8a–c. EAE mice also had significantly reduced synapsin-1 expression in the pyramidal and oriens layers of CA1 (not shown). This effect was specific to MOG-induced EAE, as experiments using CFA alone did not cause decreased Syn-1 immunoreactivity in the hippocampus, data not shown. Together, these results demonstrated reduced synaptic density within the hippocampus during EAE.

Hippocampal-Dependent Learning and Memory is Affected by EAE

We next investigated whether the hippocampal pathology shown here in EAE caused a functional deficit in hippocampal-dependent learning and memory. We used the Barnes Maze, a hippocampal-dependent behavioral task, during EAE. In this behavioral task, mice must learn the spatial location of a target hole to escape noxious visual and auditory stimuli. Performance is rated as the decrease in total errors committed by each animal from the first to last trial of the day. Fewer errors indicate learning and memory of spatial location of the target hole.

Mice with early EAE (day 15) performed similarly to healthy matched controls, in the Barnes Maze. Both groups had a significant reduction in the number of total errors committed from the first trial to the last trial, Figure 9b. In other words, EAE mice were as good as age-matched healthy normal mice in learning the location of the target hole. It is interesting to note that mice with relatively late EAE (day 40) committed more errors in the last trial, than healthy control mice, Figure 9d. Together, these data indicated that EAE causes hippocampal-dependent impairment in learning and memory.

DISCUSSION

In this study, we have demonstrated that during EAE there is hippocampal neurodegeneration that consisted of decreased CA1 volume and loss of GABA-ergic interneurons. Further, CA1 neurodegeneration was associated with hippocampal-dependent dysfunction in learning and memory during a spatial task. We then determined the cellular basis underlying CA1 atrophy, and began by assessing inflammation and demyelination, classic hallmarks of EAE pathology. It is interesting to note that we found increased microglial activation, but a relative paucity of inflammatory infiltrates. We also found diffuse demyelination with out significant axonal loss. In addition, EAE mice had an increase in apoptosis of neurons, interneurons and astrocytes, as well as a significant decrease in synaptic puncta. Together, our findings demonstrate that the hippocampus is targeted during autoimmune-mediated demyelinating disease.

Little is known about the causes of cognitive deficits in MS patients. Only recently, have investigators begun focusing research on the neuropathology that occurs in the cortex and subcortical regions of the brain in MS. Much of this research has been done using imaging techniques, such as MRI. Region-specific hippocampal atrophy has recently been reported, using high resolution T2-weighted MRI scanning, in conjunction with stringent sub-region volume analyses.[15] MS patients had significantly atrophied hippocampi, as measured by total hippocampal volume. When hippocampal sub-regions were analyzed independently, a significant reduction was detected in the CA1 of early stage MS patients, with further regional worsening of CA23/dentate gyrus (DG) in late stage MS patients. Reported volume loss analyses were correlated with impaired performance on a word-learning task, but not on an information-processing speed test, the Paced Auditory Serial Addition Task (PASAT).[15] In addition, a histopathological study described a selective decrease in neuronal numbers within the CA1 and CA2-3, which correlated with total hippocampal atrophy in MS patients,

compared with age-matched healthy controls.29 Together, these two recent studies confirm that hippocampal pathology occurs during MS. Our findings in EAE, an animal model of MS, are consistent with the observations in MS. We have identified and characterized neurodegeneration of the hippocampus, and subsequent functional impairment of hippocampal-dependent learning and memory. With these data, we propose that EAE is a model of hippocampal degeneration and dysfunction in a setting of autoimmune demyelinating disease. This model can now be used to explore preclinical treatments targeted toward preventing this neuropathology and dysfunction.

We detected apoptosis within the CA1 of EAE mice, which primarily occurred in pyramidal neurons and astrocytes. In several neurodegenerative diseases, apoptosis can occur early in response to mitochondrial dysfunction, oxidative stress and reduced synaptic transmission.[30] As the brain region governs learning and memory consolidation, the hippocampus constantly receives and transmits neural signals, thereby heavily consuming energy. Energy consumption and expenditure is regulated by mitochondria, and an imbalance in cellular homeostasis could have detrimental effects on neuronal health. In EAE, activated microglial have been shown to release reactive oxidative species, which may lead to mitochondrial impairment and trigger apoptotic signaling cascades.[31] In a recent report using Wistar rats, EAE-induced inflammation caused an increase in nitric oxide metabolites and a decrease in choline acetyl transferase in the hippocampus. [32] These data are consistent with our detection of apoptosis within the CA1 of the hippocampus during EAE in C57BL/6 mice.

In our study, we observed significant disruption in the immunoreactivity and structural integrity of synapses within the pyramidal and oriens layer of the CA1. These layers contained significant microglial activation, but were not characterized by classic focal infiltrating lesions, such as those that occur in the spinal cord WM in EAE. Previously, in rat and guinea pig models of EAE, dendritic and synaptic pathology were reported in the lumbosacral gray matter of the spinal cord.[33] Pathology was characterized by dendritic beading and swelling in WM and loss of synaptic protein expression in both WM and gray matter. These effects were correlated with inflammatory cell infiltration in the lumbosacral spinal cord. It must be noted that cortical brain regions were not assessed in that study and synaptic changes were not shown in the absence of infiltrating inflammatory cells. In a mouse EAE model, dendritic abnormalities have also been reported in motor neurons within the lumbosacral spinal cord in EAE, again in the presence of local infiltrating inflammation.[34]

Several reports have indicated that activated resident microglia have a role in neuronal injury during MS and EAE,[35] and microglial activation has been correlated with cortical and callosal neuropathology as well as with synaptic stripping in EAE.36 In a recent study, EAE-induced inflammation was shown to trigger synaptic pathology in the striatum of mice, and this study suggested that altered glutamatergic transmission is involved.37 As synaptic organization is dependent upon extracellular matrix proteins and cell adhesion molecules, 38 another study investigated whether cell adhesion molecules might be involved in synaptic pathology in the rat brain during EAE.[39] Matrix metalloproteinase-2 (MMP-2) was increased and neural cell adhesion molecule-1 (NCAM-1) was decreased within the CA1 and CA3 fields of the hippocampus. Our new findings in the context of these previous studies provide strong evidence of synaptic pathology in EAE, with our study focusing on a new region, the hippocampus. Furthermore, we provide a functional consequence of disrupted synaptic integrity, where EAE mice showed impaired performance in a hippocampal-dependent spatial memory task.

Hippocampal pathology is common in other neurodegenerative diseases, such as Alzheimer's disease (AD), HIV-1 associated dementia (HAD), epilepsy and stroke, and their

respective animal models.[40–44] The etiology and pathogenesis of each disease is distinct; however, the hippocampus is targeted in all. Furthermore, these neurodegenerative diseases share a common neuropathological element, that of abnormal synapses. The CA1 field is highly vulnerable to glutamate-mediated excitotoxicity,[45] and has been found to undergo delayed neuronal death and dysfunctional synaptic protein expression in animal models of stroke.[46–49] Here, for the first time, we report significant decreases in synaptic integrity within the CA1 during EAE, thereby suggesting that similar neurodegenerative mechanisms may be shared between diseases which are disparate in etiology. Furthermore, strategies used to prevent neuropathology in other diseases may warrant investigation in EAE.

In conclusion, our data demonstrate that the hippocampus is targeted during EAE. Our findings suggest that synaptic pruning and neuronal loss are key components in the breakdown of hippocampal integrity in the MS model. This report provides novel targets for future therapies aimed at preventing hippocampal neuropathology in MS.

Acknowledgments

This work was supported by grants RG 3593, RG 4033 and CA 1028 from the National Multiple Sclerosis Society to RRV and the Skirball Foundation. MZ is a trainee of the UCLA Laboratory of Neuroendocrinology (LNE), funded by NIH T32 HD07228-26. The authors would like to acknowledge Ms. Sienmi Du for her technical assistance and contribution to this work. Supported by the NIH (RO1 NS45443, Training Grant to MZ, 5-T32-HD07228-26) and the National Multiple Sclerosis Society (grants RG 3593, RG 4033, and CA 1028) to RRV.

References

1. Vyse TJ, Todd JA. Genetic analysis of autoimmune disease. Cell 1996;85:311–318. [PubMed: 8616887]
2. Hemmer B, Nessler S, Zhou D. Immunopathogenesis and immunotherapy of multiple sclerosis. Nat Clin Pract Neurol 2006;2:201–211. [PubMed: 16932551]
3. Dutta R, Trapp BD. Pathogenesis of axonal and neuronal damage in multiple sclerosis. Neurology 2007;68 Supp 3(22):S22–S31. [PubMed: 17548565]
4. Bö L, Geurts JJ, Mörk SJ, et al. Grey matter pathology in multiple sclerosis. Acta Neurol Scand 2006;183 Suppl:48–50.
5. Cifelli A, Arridge M, Jezzard P, et al. Thalamic neurodegeneration in multiple sclerosis. Ann Neurol 2002;52:650–653. [PubMed: 12402265]
6. De Stefano N, Narayanan S, Francis GS. Evidence of axonal damage in the early stages of multiple sclerosis and its relevance to disability. Arch Neurol 2001;58:65–70. [PubMed: 11176938]
7. Filippi M, Bozzali M, Rovaris M. Evidence for widespread axonal damage at the earliest clinical stage of multiple sclerosis. Brain 2003;126:433–437. [PubMed: 12538409]
8. Ge Y, Grossman RI, Udupa JK. Brain atrophy in relapsing-remitting multiple sclerosis and secondary progressive multiple sclerosis: longitudinal quantitative analysis. Radiology 2000;214:665–670. [PubMed: 10715027]
9. Lisak RP. Neurodegeneration in multiple sclerosis: defining the problem. Neurol 2007;68:S5–S12.
10. Magnano I, Aiello I, Piras MR. Cognitive impairment and neurophysiological correlates in MS. J Neurol Sci 2006;245:117–122. [PubMed: 16697015]
11. Amato MP, Bartolozzi ML, Zipoli V, et al. Neocortical volume decrease in relapsing-remitting MS patients with mild cognitive impairment. Neurology 2004;63:89–93. [PubMed: 15249616]
12. Rao SM. Neuropsychology of multiple sclerosis. Curr Opin Neurol 2001;8:216–220. [PubMed: 7551121]
13. Drake MA, Carra A, Allegri RF, et al. Differential patterns of memory performance in relapsing, remitting and secondary progressive multiple sclerosis. Neurol India 2006;54:370–376. [PubMed: 17114845]
14. Paulesu E, Perani D, Fazio F. Functional basis of memory impairment in multiple sclerosis: a [18F] FDG PET study. Neuroimage 1996;4:87–96. [PubMed: 9345500]

15. Sicotte N, Kern KC, Giesser BS. Regional hippocampal atrophy in multiple sclerosis. Brain 2008;131:1134–1141. [PubMed: 18375977]
16. Wujek JR, Bjartmar C, Richer E. Axon loss in the spinal cord determines permanent neurological disability in an animal model of multiple sclerosis. J Neuropathol Exp Neurol 2002;61:23–32. [PubMed: 11829341]
17. Fuss B, Afshari FS, Colello RJ, et al. Normal CNS myelination in transgenic mice overexpressing MHC class I H-2L(d) in oligodendrocytes. Moll Cell Neurosci 2001;18:221–234.
18. Mallon BS, Macklin WB. Overexpression of the 3′-untranslated region of myelin proteolipid protein mRNA leads to reduced expression of endogenous proteolipid mRNA. Neurochem 2002;27:1349–1360.
19. Liu H, Loo KK, Palaszynski K, et al. Estrogen receptor {alpha} mediates estrogen's immune protection in autoimmune disease. J Immunol 2003;171:6936–6940. [PubMed: 14662901]
20. Morales LBJ, Loo KK, Liu HB, et al. Treatment with an estrogen receptor {alpha} ligand is neuroprotective in experimental autoimmune encephalomyelitis. J Neurosci 2006;26:6823–6833. [PubMed: 16793889]
21. Pettinelli C, McFarlin DE. Adoptive transfer of experimental allergic encephalomyelitis in SJL/J mice after *in vitro* activation of lymph node cells by myelin basic protein: requirement for Lyt 1+ 2- T lymphocytes. J Immunol 1981;127:1420–1423. [PubMed: 6168690]
22. Ping SE, Trieu J, Wlodef ME, et al. Effects of estrogen on basal forebrain cholinergic neurons and spatial learning. J Neurosci Res 2008;86:1588–1598. [PubMed: 18431813]
23. Barrett GL, Bennie A, Trieu J, et al. The chronology of age-related spatial learning impairment in two rat strains, as tested by the Barnes Maze. Beh Neurosci 2009;123:533–538.
24. Gundersen HJ, Jensen EB. The efficiency of systematic sampling in stereology and its prediction. J Microsc 1987;147:229–263. [PubMed: 3430576]
25. Cruz-Orive LM. Precision of Cavalieri sections and slices with local errors. J Microsc 1999;193:182–198. [PubMed: 10348655]
26. Paxinos, G.; Franklin, KBJ. The Mouse Brain in Stereological Coordinates. 2 ed. San Diego, CA: Academic Press; 2001.
27. Rasband, W. Grid Plug-in NIH. 2001. http://rsb.info.nih.gov/ij/plugins/grid.html,
28. Zlokovic B. The blood-brain barrier in health and chronic neurodegenerative disorders. Neuron 2008;57:178–201. [PubMed: 18215617]
29. Papadopoulos D, Dukes S, Patel R. Substantial archaecortical atrophy and neuronal loss in multiple sclerosis. Brain Pathol 2009;19:238–253. [PubMed: 18492094]
30. Keating D. Mitochondrial dysfunction, oxidative stress, regulation of exocytosis and their relevance to neurodegenerative diseases. J Neurochem 2008;104:298–305. [PubMed: 17961149]
31. Stahnke T, Stadelmann C, Netzler A. Differential upregulation of heme oxygenase-1 (HSP32) in glial cells after oxidative stress and in demyelinating disorders. J Mol Neurosci 2007;32:25–37. [PubMed: 17873285]
32. Sajad M, Zargan J, Chawla R, et al. Hippocampal neurodegeneration in experimental autoimmune encephalomyelitis (EAE): potential role of inflammation activated myeloperoxidase. Mol Cell Biochem 2009;328:183–188. [PubMed: 19301098]
33. Zhu B, Luo L, Moore GRW. Dendritic and synaptic pathology in experimental autoimmune encephalomyelitis. Am J Pathol 2003;162:1639–1650. [PubMed: 12707048]
34. Bannerman PG, Hahn A, Ramirez S, et al. Motor neuron pathology in experimental autoimmune encephalomyelitis: studies in THYI-YFP transgenic mice. Brain 2005;128:1877–1886. [PubMed: 15901645]
35. Heppner FL, Greter M, Marino D. Experimental autoimmune encephalomyelitis repressed by microglial paralysis. Nat Med 2005;11:146–152. [PubMed: 15665833]
36. Rasmussen S, Wang Y, Kivisakk P. Persistent activation of microglia is associated with neuronal dysfunction of callosal projecting pathways and multiple sclerosis-like lesions in relapsing remitting experimental autoimmune encephalomyelitis. Brain 2007;130:2816–2829. [PubMed: 17890734]

37. Centonze D, Muzio L, Rossi S, et al. Inflammation triggers synaptic alteration and degeneration in experimental autoimmune encephalomyelitis. J Neurosci 2009;29:3442–3452. [PubMed: 19295150]
38. Bahr BA, Staubli U, Xiao P, et al. Arg-Gly-Asp-Ser-selective adhesion and the stabilization of long-term potentiation: pharmacological studies and the characterization of a candidate matrix receptor. J Neurosci 1997;17:1320–1329. [PubMed: 9006975]
39. Jovanova-Nesic K, Shoenfeld Y. MMP-2, VCAM-1 and NCAM-1 expression in the brain of rats with experimental autoimmune encephalomyelitis as a trigger mechanism for synaptic plasticity and pathology. J Neuroimmunol 2006;181:112–121. [PubMed: 17064783]
40. Bell K, Bennett DA, Cuello AC. Paradoxical upregulation of glutamatergic presynaptic boutons during mild cognitive impairment. J Neurosci 2007;27:10810–10817. [PubMed: 17913914]
41. Bellizzi MJ, Lu SM, Gelbard HA. Protecting the synapse: evidence for a rational strategy to treat HIV-1 associated neurologic disease. J Neuroimmune Pharmacol 2006;1:20–31. [PubMed: 18040788]
42. Poluektova L, Meyer V, Walters L. Macrophage-induced inflammation affects hippocampal plasticity and neuronal development in a murine model of HIV-1 encephalitis. Glia 2005;52:344–353. [PubMed: 16078235]
43. Zhang X, Cui SS, Wallace AE. Relations between brain pathology and temporal lobe epilepsy. J Neurosci 2002;22:6052–6061. [PubMed: 12122066]
44. MacDonald JF, Xiong ZG, Jackson MF. Paradox of Ca2+ signaling, cell death and stroke. Trends Neurosci 2006;29:75–81. [PubMed: 16376999]
45. Curtis MA, Faull RLM, Eriksson PS. The effect of neurodegenerative diseases on the subventricular zone. Nat Rev Neurosci 2007;8:712–723. [PubMed: 17704813]
46. Ouyang Y, Voloboueva LA, Xu LJ, et al. Selective dysfunction of hippocampal CA1 astrocytes contributes to delayed neuronal damage after transient forebrain ischemia. J Neurosci 2007;27:4253–4260. [PubMed: 17442809]
47. Brown CE, Wong C, Murphy TH. Rapid morphologic plasticity of periinfarct dendritic spines after focal ischemic stroke. Stroke 2006;39:1286–1291. [PubMed: 18323506]
48. Yamashiro K, Liu R, Maeda M. Induction and selective accumulation of mutant ubiquitin in CA1 pyramidal neurons after transient global ischemia. Neuroscience 2007;147:71–79. [PubMed: 17512670]
49. Lee SR, Lok J, Rosell A, et al. Reduction of hippocampal cell death and proteolytic responses in tissue plasminogen activator knockout mice after transient global cerebral ischemia. Neuroscience 2007;150:50–57. [PubMed: 17936515]

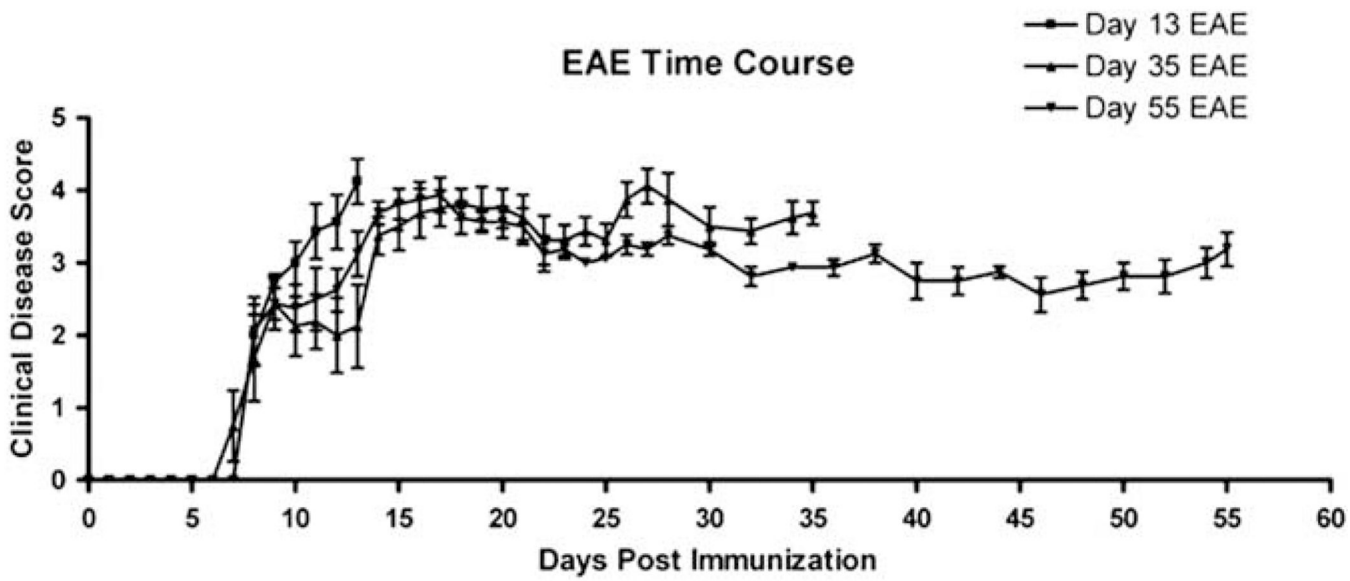

Figure 1.

Clinical disease scores of mice with experimental autoimmune encephalomyelitis (EAE). EAE was experimentally induced in adult C57Bl/6 mice by myelin oligodendrocyte glycoprotein (MOG) immunization at days 0 and 7. Clinical signs began as early as day 7. Mice were sacrificed at early (day 13; $n = 8$) middle (day 35; $n = 8$) and late (day 55; $n = 8$) disease time points, in order to assess neuropathology in the hippocampus.

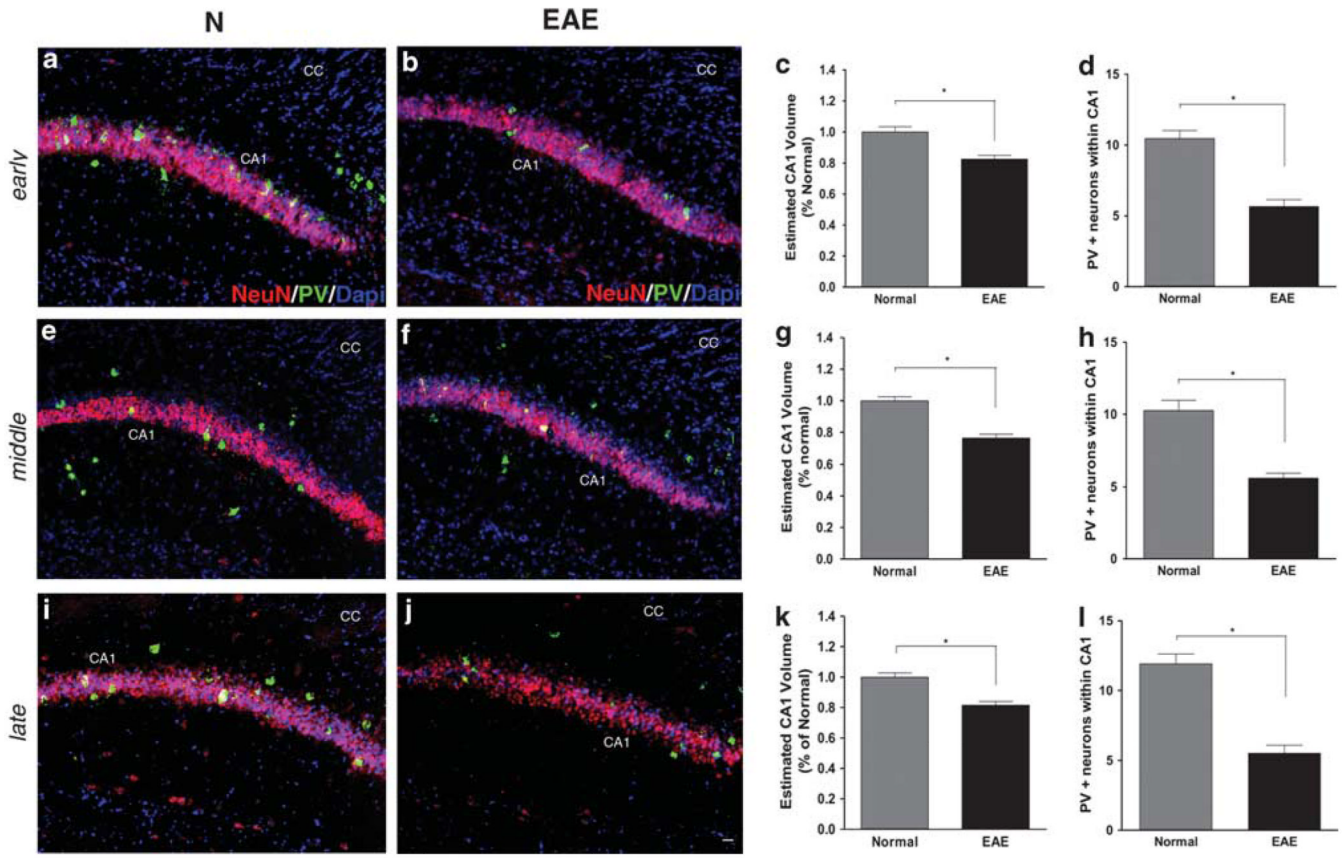

Figure 2.

CA1 pathology in experimental autoimmune encephalomyelitis (EAE) includes decreases in pyramidal volume and numbers of GABA-ergic interneurons. Decreased pyramidal layer volume and interneuron loss occur in EAE mice at early (**b**), middle (**f**) and late (**j**) stages of disease, compared with gender and age-matched healthy mice (**a**, **e** and **i**). All panels are pseudo-colored confocal images taken at × 10 magnification. CA1 neurons (NeuN, Cy5-red), GABA-ergic interneurons (parvalbumin (PV), FitC-green) and cell nuclei (DAPI, blue) are depicted in images. Quantification of decreased pyramidal CA1 volume (**c, g** and **k**) and interneurons (**d**, **h** and **l**) at each time point of EAE shown to the right in graphs. *Denotes statistical significance compared with normal, (P<0.001); Student's t test, n = 8 per condition, per time point. Subsequent experiments have confirmed these results. Scale bar, 20 μm.

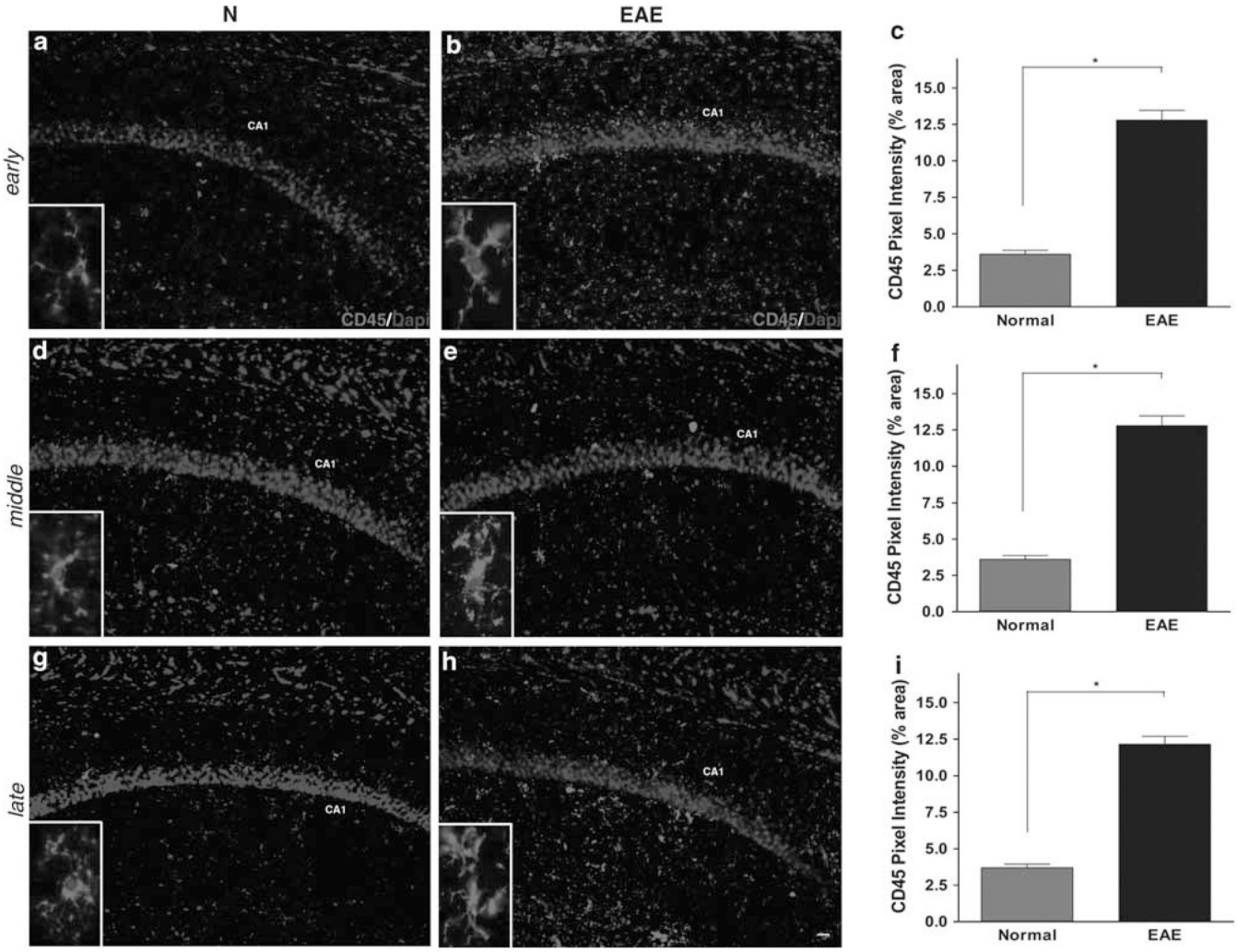

Figure 3.

Inflammation in the hippocampal CA1 region during experimental autoimmune encephalomyelitis (EAE). Microglial activation, identified by CD45+ labeling (Cy5-red), was measured in dorsal CA1 of early-, middle- and late-stage EAE mice, and compared with healthy age-matched normal mice. Normal mice and EAE mice are denoted by N and EAE. At all time points, EAE mice had significantly more CD45+ labeling than normal mice. CA1 seen by DAPI+ labeling (blue) of pyramidal cell layer. Images were taken at × 10 magnification, with small insets of normal and activated microglia, taken at × 40 magnification. Microglia in EAE have ramified morphology, indicative of inflammatory activation. Quantification of CD45+ pixel intensity (% area of immunoreactivity) shown in graphs **c, f** and **i**, with *indicating statistical significance, $P<0.0001$; $n = 8$ per condition, per time point. Scale bar, 20 μm.

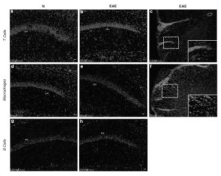

Figure 4.
Hippocampal inflammation is not due to infiltrating T and B lymphocytes. At early time points, the hippocampus of normal and experimental autoimmune encephalomyelitis (EAE) mice did not stain for CD3 or CD19+ cells (Cy5-red), which label T cells and B cells, respectively (**a**, **b**, **g**, **h**). However, there was some macrophage/monocyte labeling seen in the CA1 of EAE mice (**e**) compared to normal mice (**d**). As a positive control for the ability to detect immune cell infiltration, thoracic spinal cord sections from EAE animals revealed both CD3+ and macrophage+ staining, (Cy5-red) (**c** and **f**). Sections were double-labeled for each antibody in conjunction with DAPI (blue), a nuclear DNA cell marker, and imaged at × 10 magnification using confocal microscopy. CA1 pyramidal layer is identified. Scale bar, 20 μm.

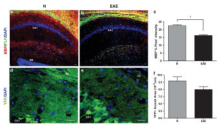

Figure 5.

Widespread reduction of myelin in hippocampus during experimental autoimmune encephalomyelitis (EAE). Myelin basic protein (MBP, Cy5-red) staining was significantly reduced in the hippocampus of EAE mice (**b**), compared with normal control mice (**a**). Quantification of myelin pixel intensity depicted in graph c, where * indicates statistical significance, ($P<0.001$, Student's *t* test). Confocal images shown are taken at × 10 magnification from PLP-EGFP tissue sections, where PLP+ oligodendrocytes express EGFP (green), and cell nuclei are stained with DAPI (blue). EAE mice did not have significantly less PLP+ oligodendrocytes in the CA1 compared with normal mice (**a, b**). Tissue sections from Thy1-YFP (YFP-green) normal and EAE mice were stained with cell nuclei marker, DAPI (blue) to assess axonal area (**d**–**e**). To assess CA1 axons specifically, the stratum oriens was analyzed, ('SO' in panels). EAE mice did not have significantly different CA1 axonal area (**e**), compared with healthy normal control mice (**d**). Quantification is shown in graph **f**, where a Student's t test yielded non-significant differences in CA1 axonal area, $P>0.05$. Scale bars, 20 μm.

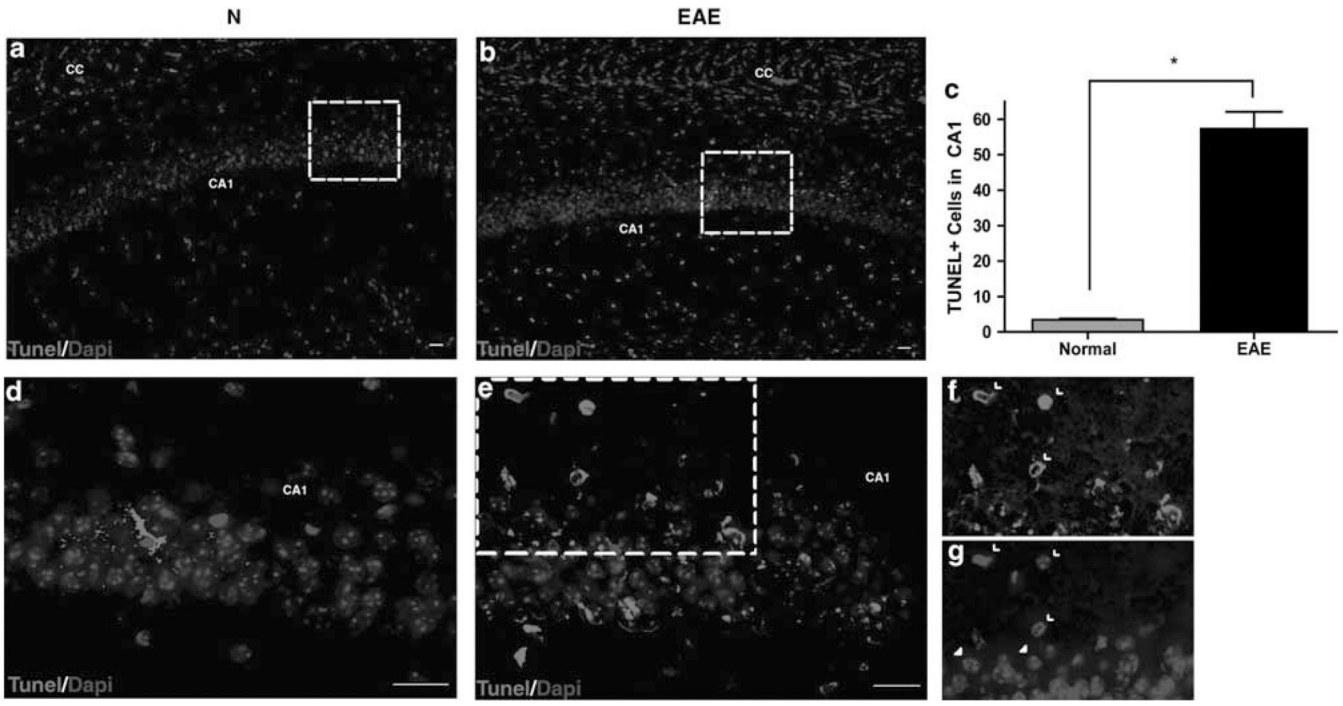

Figure 6.

Increased cell death in the CA1 region of experimental autoimmune encephalomyelitis (EAE) mice. EAE mice had significantly more TUNEL+ cells in all layers of rostral CA1 (**b** and **e**), compared with normal control mice (**a** and **d**). TUNEL+ labeling (TMR-red) and cell nuclei (DAPI-blue) within CA1 are shown in × 10 confocal images (**a** and **b**) in normal and EAE mice. There were significantly more cells undergoing apoptosis in EAE mice compared with normal mice, quantification in graph (**c**). *Statistically significant, $P<0.0001$, Student's unpaired t test, $n = 8$ per condition. **d** and **e** are × 40 magnified images representative of dashed squares in corresponding × 10 images. **f** and **g** are color split images of **e**. TUNEL+ cells are indeed DAPI+ (open arrow heads); however, not all DAPI+ cells are TUNEL+ (closed arrow heads). All scale bars are 20 μm.

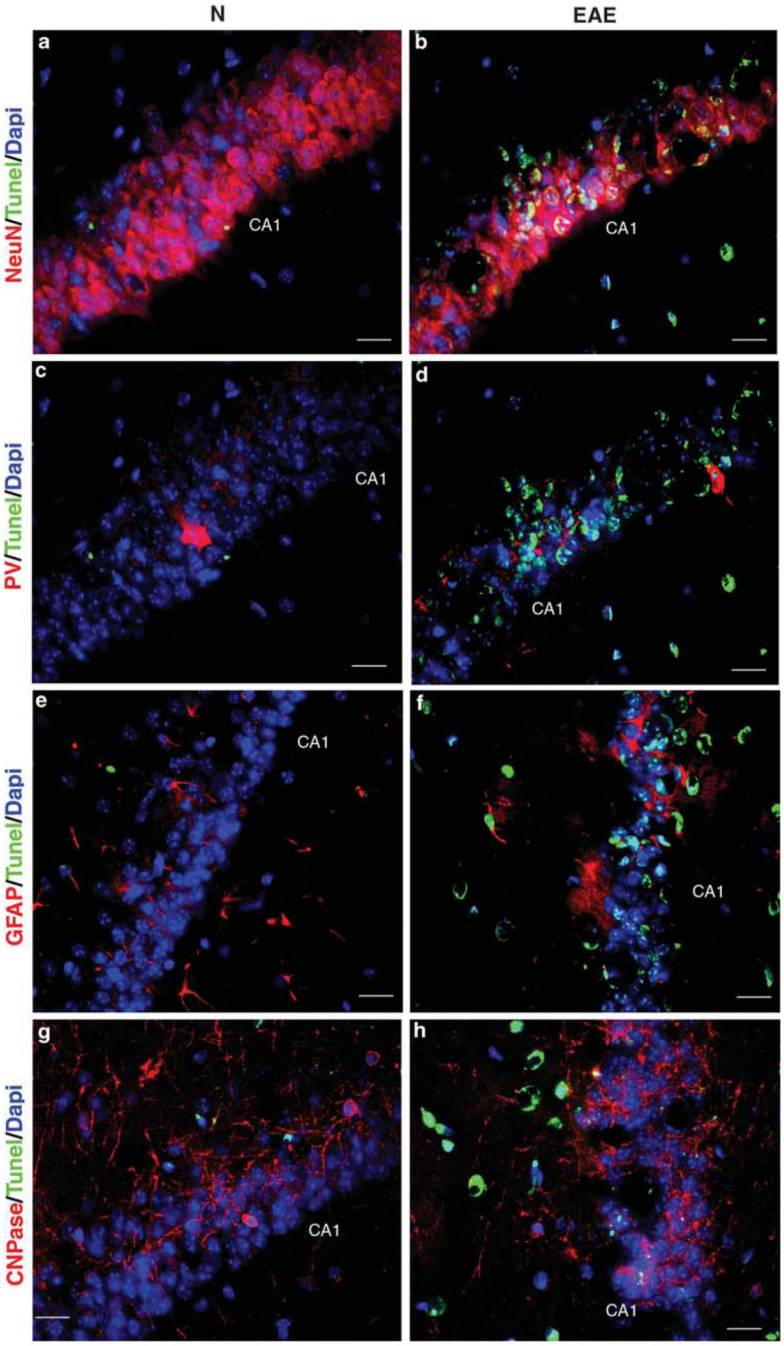

Figure 7.

CA1 cell death occurs primarily in neurons and astrocytes, and occasionally in GABA-ergic interneurons and oligodendrocytes. Co-labeling experiments were used to identify the various cell types undergoing apoptosis in the CA1 of experimental autoimmune encephalomyelitis (EAE) mice. All panels depict × 40 magnified images of the dorsal CA1 of normal and EAE mice at early stages of disease. TUNEL+ cells are shown in pseudo-colored green in all panels, whereas each specific cell marker is red. Normal CA1 had sporadic TUNEL+ cells, and normal NeuN+ (**a**), PV+ (**c**), GFAP+ (**e**) and CNPase+ (**g**) labeling. The CA1 of EAE mice; however, showed significantly more TUNEL+ staining

which co-labeled with NeuN (**b**), parvalbumin (PV) (**d**), GFAP (**f**) and relatively few CNPase co-labeling (**e**). All scale bars are 20 μm.

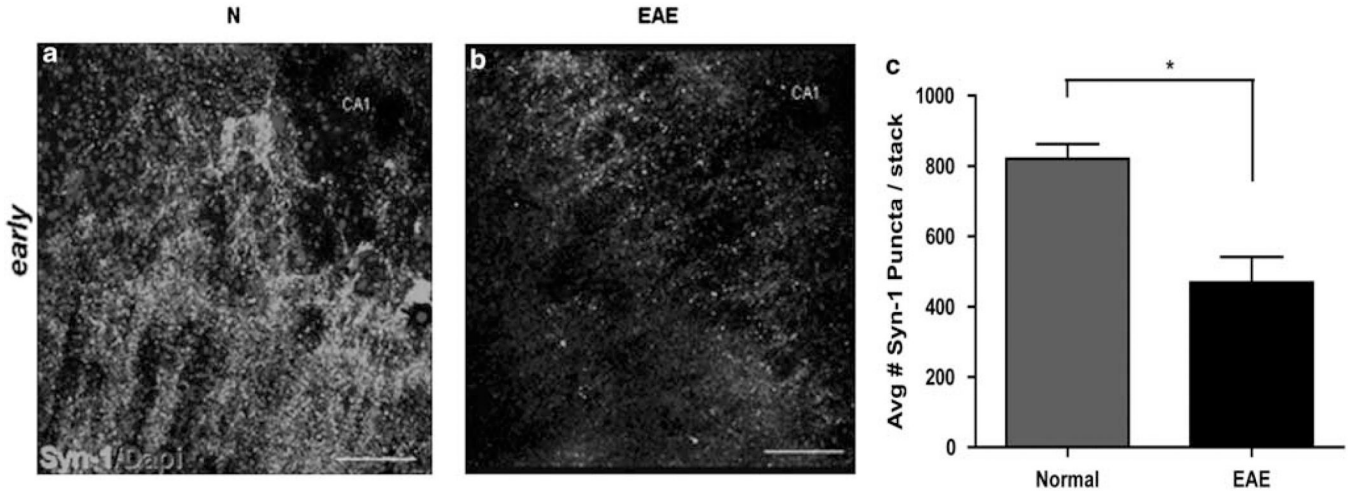

Figure 8.

Synaptic loss in the CA1 region of experimental autoimmune encephalomyelitis (EAE) mice. Decreased synaptic protein, synapsin-1 (Syn-1; FitC-green) was observed in stratum radiatum, stratum pyramidale and stratum oriens of EAE mice (day 13, **b**) compared with healthy age-matched normal mice (**a**). Both immunoreactivity and quantity of synaptic puncta were significantly decreased in EAE hippocampus. Normal and EAE mice indicated by N and EAE in left and right columns. **a** and **b** depict dorsal CA1 cells (DAPI-blue) and Syn-1 immunoreactivity at high magnification, × 100, scale bar 20 μm. Graph (**c**) represents average number of Syn-1 immunoreactive puncta counted per stack, where EAE CA1 had approximately 40% decreased number of puncta compared with healthy control, **P*<0.005, Student's *t* test, *n* = 4 per condition.

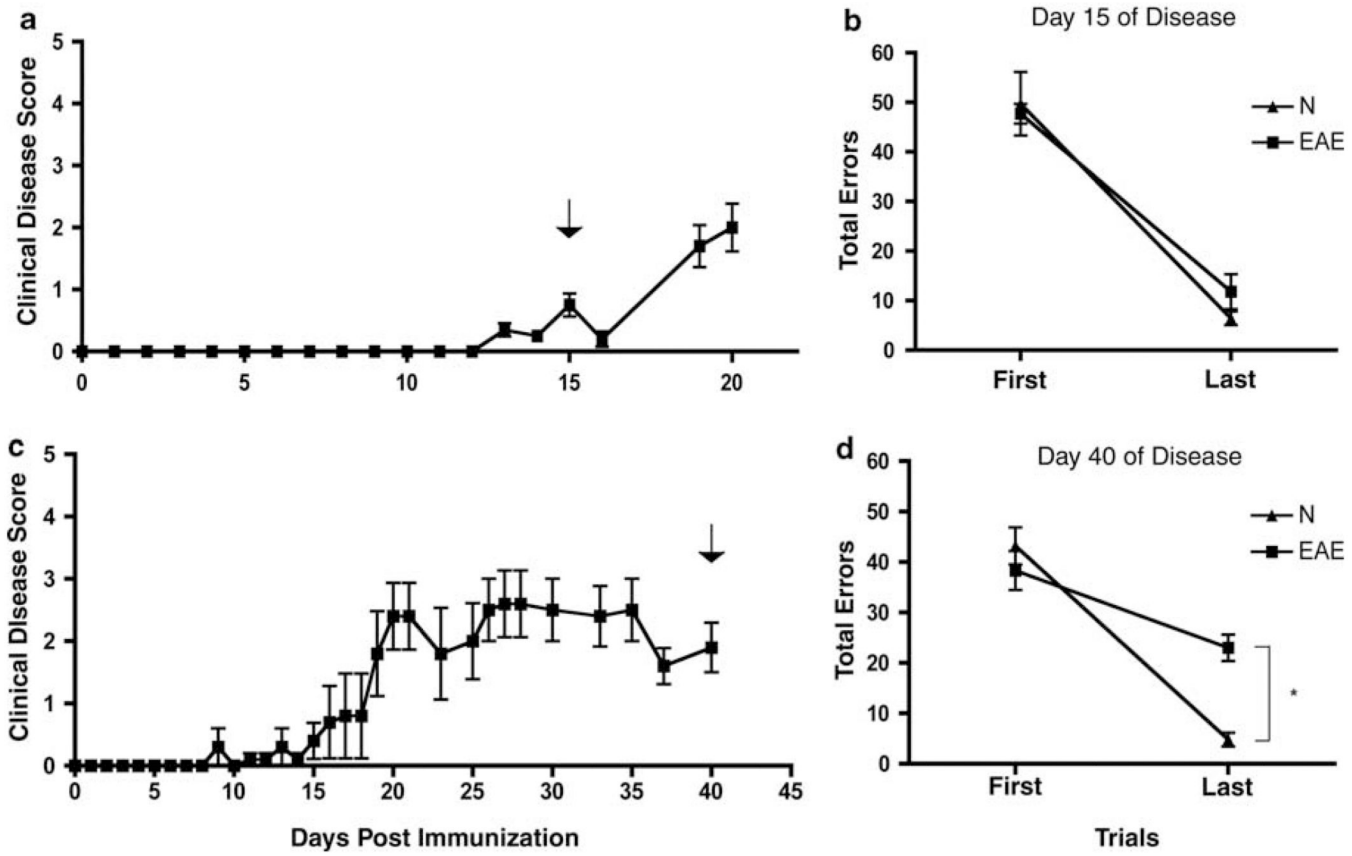

Figure 9.

Experimental autoimmune encephalomyelitis (EAE) causes a deficit in hippocampal-dependent spatial learning and memory at a later stage of disease. Spatial learning and memory was assessed in normal and EAE mice at two time points of disease (days 15 and 40). Graphs (**a**) and (**c**) show representative clinical disease courses for mice tested at an early time point (day 15), and mice tested at a later time point (day 40). On each test day, mice were each given three 300 s trials, in which they were to learn the location of a target hole in the Barnes Maze, and escape from noxious stimuli. Trials terminated at end of 300 s or when mouse entered target hole and escaped to target cage. Errors were defined as explorations into incorrect holes, and were counted and summed for each individual, then averaged by group to give total errors. At an early time point EAE and age-matched healthy control mice performed similarly in the Barnes Maze test, where both groups successfully committed fewer errors by the last trial of the day, graph (**b**). Later in disease, however, EAE mice had impaired performance, and committed significantly more errors during the last trial, than age-matched healthy controls, graph (**d**). Repeated-measures ANOVA yielded significant difference (*) after pair-wise comparisons, $P<0.008$; Bonferroni post-hoc analysis indicated significant difference between normal and EAE mice during last trial, $P<0.01$.